

# Xstrings: 3D Printing Cable-driven Mechanism for Actuation, Deformation, and Manipulation

Jiaji Li  
jiaji@mit.edu  
MIT CSAIL  
Cambridge, MA, USA  
Zhejiang University  
Hangzhou, China

Shuyue Feng  
shuyuefeng@zju.edu.cn  
Zhejiang University  
Hangzhou, China

Maxine Perroni-Scharf  
max1@mit.edu  
MIT CSAIL  
Cambridge, MA, USA

Yujia Liu  
liuyujia@tsinghua.edu.cn  
Tsinghua University  
Beijing, China

Emily Guan  
emilyguan@pratt.edu  
Pratt Institute  
Brooklyn, NY, USA

Guanyun Wang  
guanyunwang@zju.edu.cn  
Zhejiang University  
Hangzhou, China

Stefanie Mueller  
stefaniem@csail.mit.edu  
MIT CSAIL  
Cambridge, MA, USA

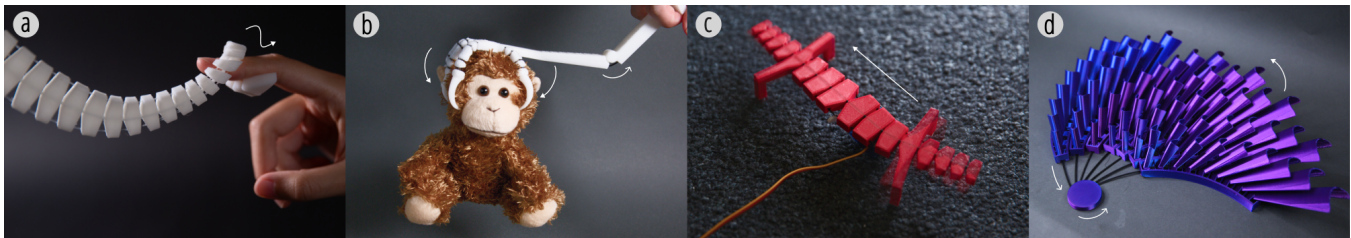


**Figure 1:** Four 3D-printed objects demonstrating applications of Xstrings, including (a) multi-directional tentacle manipulation, (b) a claw with embedded actuation, (c) a bio-inspired lizard robot, and (d) a dynamic wall sculpture.

## ABSTRACT

In this paper, we present Xstrings, a method for designing and fabricating 3D printed objects with integrated cable-driven mechanisms that can be printed in one go without the need for manual assembly. Xstrings supports four types of cable-driven interactions—bend, coil, screw and compress—which are activated by applying an input force to the cables. To facilitate the design of Xstrings objects, we present a design tool that allows users to embed cable-driven mechanisms into object geometries based on their desired interactions by automatically placing joints and cables inside the object. To assess our system, we investigate the effect of printing parameters on the strength of Xstrings objects and the extent to which the interactions are repeatable without cable breakage. We demonstrate the application potential of Xstrings through examples such as manipulable gripping, bionic robot manufacturing, and dynamic prototyping.

## CCS CONCEPTS

• **Human-centered computing** → **Human computer interaction (HCI)**; **Systems and tools for interaction design**.

## KEYWORDS

Cable-driven Mechanism, Personal Fabrication, 3D Printing

### ACM Reference Format:

Jiaji Li, Shuyue Feng, Maxine Perroni-Scharf, Yujia Liu, Emily Guan, Guanyun Wang, and Stefanie Mueller. 2025. Xstrings: 3D Printing Cable-driven Mechanism for Actuation, Deformation, and Manipulation. In *CHI Conference on Human Factors in Computing Systems (CHI '25)*, April 26-May 1, 2025, Yokohama, Japan. ACM, New York, NY, USA, 18 pages. <https://doi.org/10.1145/3706598.3714282>

## 1 INTRODUCTION

Prior HCI research has focused on integrating mechanisms into physical objects to enable the creation of dynamic, articulated, and shape-changing structures. To achieve different types of dynamic interactions, researchers have explored various mechanisms to support compliant [28, 53], elastic [13, 43, 48], bi-stable [39, 61], and shape-memory [32, 42] fabrication, allowing users to customize dynamic devices and tangible interfaces.

Please use nonacm option or ACM Engage class to enable CC licenses. This work is licensed under a Creative Commons Attribution-NonCommercial 4.0 International License.



*CHI '25*, April 26-May 1, 2025, Yokohama, Japan  
© 2025 Copyright held by the owner/author(s).  
ACM ISBN 979-8-4007-1394-1/2025/04  
<https://doi.org/10.1145/3706598.3714282>

In parallel, cable-driven mechanisms have emerged as a cornerstone of modern robotics, where the delicate interplay of cables to transmit forces and motions offers a unique blend of precision and adaptability. Their inherent lightweight nature and flexibility make them indispensable in diverse applications, ranging from robotic actuation [44] to the development of intricate control systems [46]. For instance, Nikafrooz et al. [35] designed a robotic hand with cables embedded in each finger to mimic the function of tendons, while Colan et al. [4] leveraged similar principles in crafting advanced surgical tools.

Despite their advantages, cable-driven mechanisms can be inherently challenging to design for less experienced 3D-printing users. Achieving a specific desired motion requires precise positioning of cables and their connection points within the geometry of a larger structure, as well as the careful adjustment of tension levels in these cables. To streamline the design process of such complex mechanisms, researchers have developed various optimization algorithms. For example, Megaro et al. [27] and Li et al. [22] introduced optimization-based methods for the inverse design of cable-driven kinematic chains and trees. These methods have demonstrated the capability to generate a wide range of output motions, including realistic character animations and the development of actuated grippers, thereby expanding the versatility and application potential of cable-driven systems.

Although existing design tools provide optimization solutions for cable layouts to achieve the desired motion of an object, the fabrication of such cable-driven mechanisms remains a challenging manual task. This process often involves creating numerous small holes, meticulously threading cables through these holes, and tying knots at precise locations, an effort that is both time-consuming and labor-intensive. Furthermore, the hand-crafted nature of these mechanisms poses significant challenges in achieving the precision required for developing systems with accurate motion trajectories, limiting reproducibility and consistency when producing identical copies of the same structure.

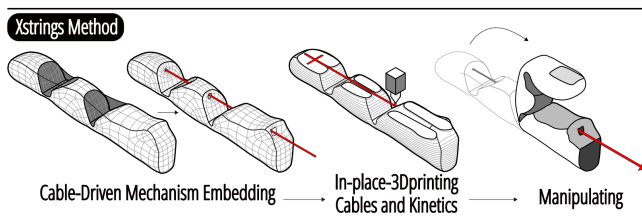


**Figure 2: Embedding cable-driven mechanism with the Xstrings workflow.**

To address these challenges, we present Xstrings, a method that integrates cable-driven mechanisms with 3D object geometries for one-step fabrication using dual-material FDM 3D printing. Xstrings supports four types of cable-driven interactions—bend, screw, coil, and compress—activated by input force on the cables. To simplify the design process, we also present a tool that allows users to embed these mechanisms into objects by automatically placing cables and joints based on the desired behavior of the object. This approach automates the creation of cable-driven mechanisms, without long

production times or manual labor, while maintaining their precision.

We evaluate Xstrings through several experiments. First, we measure its time-efficiency by comparing it to manual cable-driven object assembly over four participants, finding that Xstrings reduces assembly time by 40%. Additionally, we examine the impact of printing parameters such as temperature and speed on cable quality, testing maximum tensile strain and interaction repeatability. Finally, we showcase the potential applications of Xstrings with a diverse set of 3D-printed examples, including dynamic fashion, bionic robotics, and interactive prototyping, highlighting how Xstrings accelerates fabrication for both novice and expert users. In summary, our contributions are as follows:

- An automated, one-step fabrication approach for 3D printing cable-driven mechanisms, by printing embedded cables, objects, joints, and linkages all at once without the need for manual assembly.
- An interactive design tool that incorporates cable-driven mechanisms into a target structure by decimating it into a user-defined number of links, integrating four different motion primitives (bend, coil, screw, and compress) to approximate the target structure, and fosters creativity, exploration, and accessibility to cable-driven prints.
- A technical evaluation to determine how 3D printing parameters (printing temperature, extrusion, density, and print path) affect the fatigue and maximum tensile strain of the printed cables.
- A variety of 3D-printed example applications that demonstrate the use of Xstrings cable-driven mechanisms, including gripping devices, bionic robot manufacturing, and dynamic prototyping.

## 2 RELATED WORK

### 2.1 Manipulation Method of Dynamic Fabrications

In the field of personal fabrication, researchers have utilized digital manufacturing tools to create dynamic materials capable of achieving a wide range of movements that would typically require the creation and assembly of complex mechanical structures. There are two main aspects to this line of prior research: **dynamic structures**, which investigates how to impart mobility to objects, and **actuation methods**, which explores how to control the movement of dynamic objects under external forces.

Common dynamic structures in fabrication include springs [13, 14], joints [23, 59], linkages [18, 19, 57], hinges [36, 53], inflatable structures [47, 62], metamaterials [16, 17], and origami-based designs [33, 54]. For example, PneuUI [62] achieves various deformation patterns by arranging inflatable bladders in different configurations. Metamaterials have been 3D printed to create mechanisms that can rotate and extend, achieving effects for motion conduction and linkage [12, 16, 17]. Origami, widely used in engineering, can be employed to create structures that have strength values many times higher than those of their constituting materials through folding techniques [9]. Pop-up Print [37] uses a combination of rigid and flexible materials to allow greater freedom in shaping objects, making it suitable for more diverse applications.

Building upon dynamic structures, various actuation methods can be used for the precise execution of different control tasks. Such methods include pneumatic actuation [29, 34, 51], hydraulic actuation [30], cable-driven actuation [22, 24], and magnetic field manipulation [8, 20]. For instance, FlowIO provides a rapid prototyping platform for pneumatic actuation with an integrated pump terminal [51], while liquid pouch motors use low-boiling-point liquids (around 30°C) to achieve inflation and deflation through temperature changes [34]. ConeAct uses shape memory alloys to drive a flexible unit, enabling multi degree-of-freedom deformations [24]. ZeroN leverages spatial magnetic fields to suspend a small sphere mid-air and control its motion trajectory freely [20], and MechCircuit employs magnets to simulate various mechanical structures, such as gears and springs [8].

Xstrings expands this landscape by enabling the fabrication of over 30 types of print-in-place dynamic structures with the capability for complex motions. Xstrings utilizes one of the simplest actuation methods—tension applied to cables, which can be generated by the user’s hand or programmable devices such as stepper motors, to achieve these motions. Its low-cost, low-entry-barrier, and automatic approach to creating dynamic structures and actuation systems opens up new design possibilities for personalized manufacturing.

## 2.2 String-like Structures in 3D Printing

String-like structures such as hair, fibers, and cables have been widely utilized by HCI researchers in fabrication to enhance the physical properties of printed objects.

Several studies have focused on incorporating existing string-like materials into 3D-printed creations through post-processing methods [26], significantly enhancing functionality in areas such as shape transformation [25, 58], haptics [6], and sensing [40, 55]. For example, Rivera et al.[45] combine 3D printing and textiles to rapidly create rigid objects with embedded flexibility, as well as soft materials with added functionality. Medley[3] embeds everyday objects into 3D-printable designs to achieve a wider range of material properties. PunchPrint [6] and Hybrid Basketry [65] explore post-print processes where fibers are woven into printed objects, facilitating craftsmanship and customization. Similarly, Flex-Truss [52] proposes a cost-effective method that integrates various linear materials into 3D-printed nodes to form flexible prototypes. These studies involve manual weaving as a post-processing step using specific techniques, which can be challenging for ordinary 3D printing enthusiasts to learn. Moreover, the production of a large number of repetitive woven structures can result in significant labor costs.

Beyond embedding traditional fiber-like materials into 3D-printed objects, there is a growing interest in fabricating fiber-like structures directly from 3D printing materials. WirePrint [31] accelerates low-fidelity wireframe previews in the early stages of the design process. Cillia [38] achieves micro and fine-hair-like structures for motion conduction and aesthetic purposes. To further enhance the flexibility of the printing process and realize more types of prototypes with hair-like structures, Extruder-Turtle [41] provides a geometry library that simplifies the generation of G-code files

for printing on FDM printers. DefeXtiles [10] proposes employing under-extrusion strings to print woven textiles.

While these approaches offer rich physical properties, they do not result in the creation of motion systems or actuation mechanisms. Xstrings instead introduces a method for creating cable-driven mechanism using a specially designed 3D printing approach. This method enables the printing of “threaded points” (Section 3.3) that are both interconnected and capable of independent movement, thereby providing a vast design space.

## 2.3 Cable-Driven Mechanisms

Cable-driven mechanisms are fundamental in modern robotics due to their versatility and lightweight properties, making them suitable for diverse applications [15, 63]. Their flexibility and low weight are particularly advantageous for robotic actuation [44] and complex control systems [46].

Despite these benefits, designing cable-driven mechanisms is challenging. Achieving precise motion patterns requires careful geometric design, joint configuration, and strategic cable placement to ensure adequate torque. To address these complexities, researchers have developed various optimization algorithms. Megaro et al.[27] introduced an inverse design method that minimizes the number of cables and control forces while achieving target motions. Li et al.[22] proposed an inverse design strategy for push and pick-and-place tasks, enabling coordinated control of multiple cables. Shirafuji et al.[50] developed a method for designing non-circular pulleys that regulate joint motion by adjusting wire contact points to achieve specific movement ratios in robotic legs. Zhang et al.[64] extended this approach by designing noncircular pulleys for task-defined non-linearly coupled tendon-driven actuation, allowing a single motor to control multiple tendons in complex robotic systems.

Although existing design tools optimize cable layouts for desired motion, fabricating cable-driven mechanisms remains labor-intensive. The process typically involves precise drilling, threading cables through small holes, and securing knots at designated points, all of which require high manual skill and are prone to errors that may compromise reliability. To address these issues, the MoReCa grasper employs modular, reconfigurable joints to achieve various functions without altering the main structure [21]. OpenRST focuses on robot-assisted minimally invasive surgery (RMIS), providing an open platform for low-cost, biocompatible robotic surgical tools [4]. While these approaches improve assembly efficiency and reduce manufacturing costs, they do not fundamentally resolve the design and labor costs associated with cable and mechanical assembly.

Despite the advantages of cable-driven systems, their complex design and labor-intensive assembly highlight the need for automation. Xstrings addresses this challenge by integrating 3D printing into their fabrication. Through integrated manufacturing and advanced design tools, Xstrings enhances design efficiency, eliminates manual processing and assembly, and optimizes fabrication precision.

### 3 XSTRINGS METHOD

The creation of 3D-printed cable-driven mechanisms involves three main challenges: (1) laying out the cable along the mechanism; (2) integrating joints and anchors into the print to enable the desired motion of the main structure when the cable is activated; and (3) defining suitable 3D-printing parameters.

#### 3.1 Laying Out the Cable for the Mechanism

To begin with, we identify the key components that need to be included in an Xstrings object, referencing classic cable-driven mechanisms. Typically, there are three primary components used to connect a cable to a mechanical structure: (1) **Anchor Points**, (2) **Threaded Points**, and (3) **Exposed Points**, as illustrated in the example of a cable-driven finger in Fig. 3. Below, we introduce the characteristics of each component and provide a detailed explanation of their corresponding manufacturing techniques in Xstrings.

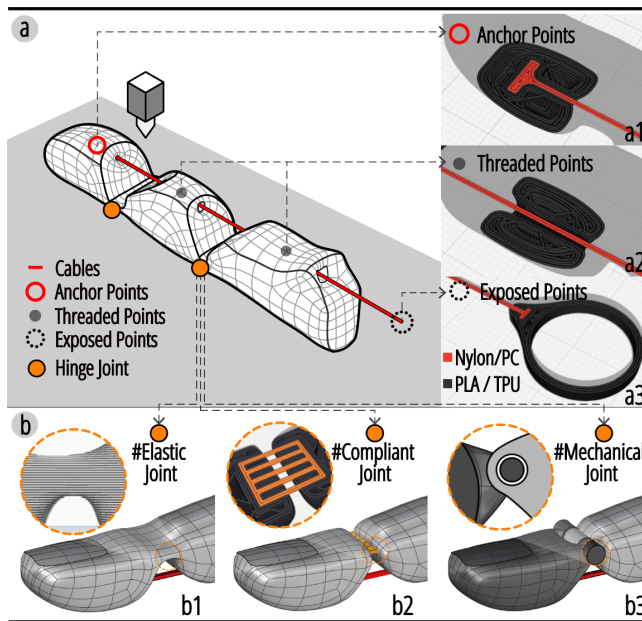


**Figure 3: (a) Three types of relationships between cables and mechanical components: Anchor Points, Threaded Points, and Exposed Points. (b) Three types of hinge joints as options: Elastic, Compliant, and Mechanical.**

**Anchor Points:** A cable-driven mechanism aims to achieve precise real-time control of the end effector (e.g., the fingertip) using cables. Traditional methods secure cables with knots, but since 3D printers cannot tie knots, we introduce an alternative anchoring method. Instead, the cable endpoint is shaped into a T-anchor and embedded within the surrounding material, as shown in Fig. 3. This design firmly secures the cable without relying on thermal adhesion between different 3D-printed materials, which may lead to separation if bonding fails [2].

**Threaded Points:** In cable-driven mechanisms, “Threaded Points” are holes in the 3D-printed structure through which a cable slides when actuated. Ensuring smooth rectilinear motion at these points is a key technical challenge. Traditionally, holes are drilled, and cables are manually threaded, but integrating this process into layer-by-layer 3D printing introduces significant issues, primarily friction and resistance between the cable and printed structure. Section 3.3 presents optimized printing parameters and materials, refined through G-code adjustments, to enhance cable quality and minimize friction.

**Exposed Points:** To actuate a cable-driven mechanism, the cable ends must be exposed for interaction. These points serve as inputs where forces are transmitted along the cable to the anchored terminal, driving the mechanism. Common actuation methods include manual pulling, motor-driven tensioning, and gravity. 3D printing enables customization of these endpoints with terminal shapes such as pull rings, spools, or solid weights to suit different interaction needs.

#### 3.2 3D Printing Joints for Cable-Driven Mechanisms

To actuate a cable-driven mechanism, there must also be some form of joint or compliance integrated into the larger 3D object being actuated. In the following subsection, we discuss three types of 3D-printed joints explored in our study.

**Elastic Joints:** 3D-printed elastic joints leverage the inherent elasticity of common 3D printing materials such as TPU and TPE. One approach to creating 3D-printable elastic joints is to modify certain areas of a 3D object printed with an elastic material to be thinner, making them capable of elastic deformation and effectively functioning as hinges. These joints can be temporarily deformed via a tensing cable and, once the tension is released, return to their original shape, releasing stored elastic energy without permanent deformation.

**Compliant Joints:** In 3D printing, compliant joints can be created by using an array of multiple thin filaments to form bridges between components of a structure. The stiffness of these filaments can be adjusted to achieve the desired amount of motion in the cable-driven mechanism [53]. Similar to elastic joints, compliant joints have the advantage of simplicity, as they eliminate the need for separate moving parts. These joints are particularly well-suited for lightweight and compact applications.

**Mechanical Joints:** Unlike elastic and compliant joints, mechanical joints rely on assembling separate, distinct moving components of a structure. In the context of 3D printing, these joints can be fabricated using a print-in-place technique [23], which allows for the creation of mechanical linkages within a single print. These mechanical joints provide robust and reliable connections between components, capable of withstanding significant loads and offering precise control over the movement of large printed components.

By exploring and combining these different types of joints, we can expand the range of applications for 3D-printed cable-actuated mechanical systems and tailor our printed objects to meet the specific needs of various scenarios.



### 3.3 3D Printing Materials and Parameters for Threading Cable

As mentioned in Section 3.1, by optimizing the print parameters and materials used for FDM 3D printing, we can create high-performance cable-actuated kinetic systems that exploit rectilinear motion between the cables and the body of the printed object. The choice of printing materials and printing parameters greatly affects the quality of the cable, which in turn impacts the motion smoothness of the entire kinetic system. As highlighted in Fig. 4b, we demonstrate that using default printing parameters leads to issues with 3D-printed cable-driven mechanisms, such as drooping and branching. Below, we discuss how we address these challenges through careful selection of print materials and optimization of G-code parameters before printing.

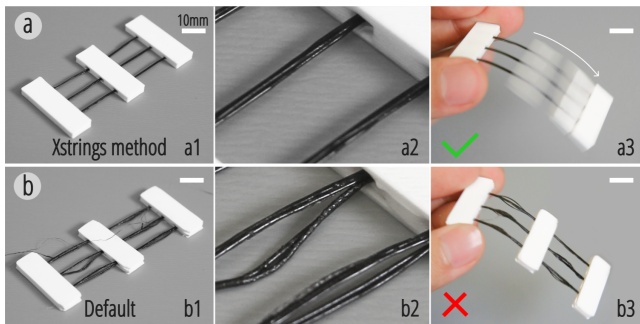


**Figure 4: (a) A 3D-printed sample using Xstrings’ G-code parameters, resulting in smooth motions of the centerpiece; (b) the same sample printed with default settings, causing the centerpiece to become stuck.**

In our cable 3D printing tests, we identified three main issues that can directly lead to failure modes:

- (1) **Fragile cables**, where the cable itself is too fragile, leading to breakage or fracture during manipulation;
- (2) **Fused materials**, where the cable and mechanical components fuse together in undesired locations due to melting during 3D printing, causing separation to become impossible, thus preventing the cable from moving and actuating the mechanism;
- (3) **Irregular shapes**, where the cable exhibits irregularities such as branching (a single cable into multiple threads, seen in Fig.4b2), uneven thickness, or sagging, which prevent it from passing through holes or result in excessive frictional resistance.

To address these issues, we take several steps as outlined below:

**Resilient Cable Materials:** Selecting the ideal material for 3D-printed cables involves balancing bending-resistance and the ability to withstand high tensile stress without undergoing plastic deformation or breakage. Based on filaments datasheets and printing guidelines, we chose Nylon and PC as test materials due to their excellent tensile properties. In practical tests, PC exhibited the highest tensile strength but was prone to plastic deformation and even

breakage under repeated bending, making it unsuitable as a cable material. Nylon, on the other hand, demonstrated exceptional bending-resistance and maintained stability and durability under repeated bending. Among different types of Nylon (carbon fiber-filled, glass fiber-filled, PA11, PA12 et al.), we selected Nylon 66 for its superior balance of flexibility and strength, making it the most suitable material for Xstrings cables.

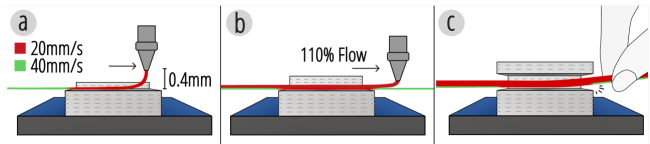


**Figure 5: Xstrings 3D printing strategies and parameters**

**Materials and Parameters to Avoid Fusion:** We print the main structure and joints using a different material than the cable to prevent fusion between the cable and surrounding geometry. If printed from a single material, the matching melting and solidification points would cause unintended bonding, making it impossible to separate components and restricting cable movement.

To mitigate this, we select materials with sufficiently different melting points [2]. We tested cable-driven mechanisms by printing cables in Nylon while using PLA and TPU for the rest of the structure. As shown in Fig. 4, these tests confirmed that cables naturally separate from their surroundings due to shrinkage or minimal manual force. Our technical evaluation (Section 8) further demonstrates that adjusting the material spacing to 0.4mm in the first cable layer via G-Code editing, setting initial layer extrusion to 90

**Printing Parameters for Cable Straightness:** During FDM 3D printing, cable sections are either suspended mid-air during extrusion or rest on previously extruded layers. We observed issues such as filament sagging and cable branching, where the cable splits into thin filaments (Fig. 4b2). These defects hinder smooth cable sliding and may obstruct passage through holes. Excessively high temperatures and slow speeds exacerbate sagging and fusion, as softened filament deforms under gravity.

To address this, we optimized 3D printing parameters through experiments (Fig. 5). For the first layer, we reduced printing speed to 20mm/s (default: 70mm/s) and set the bridging speed to 40mm/s to balance temperature and speed, minimizing drooping. The extrusion rate was adjusted to 90

**Evaluation:** We evaluated our print parameters by comparing two versions of a cable-driven mechanism consisting of a block threaded with three freely sliding cables. One sample was printed using Xstrings’ optimized G-Code parameters (Fig.4a), while the other used default printer settings (Fig.4b). Testing confirmed that our approach effectively eliminates the discussed issues, allowing smooth movement of intermediate blocks along the cables and providing reliable support for cable-driven mechanisms. Further evaluations examine cable force limits, thermal fusion of different materials, and the impact of printing parameters on cable quality through various experiments.

## 4 MOTION PRIMITIVES

In this section, we formalize four fundamental motion primitives as a foundation for automating the construction of various cable-driven 3D-printable mechanisms. In mechanical engineering, a one-degree-of-freedom (one-DOF) pair is the most basic type of mechanism that enables relative motion between two components, typically classified into Revolute, Screw, and Prismatic pairs [1]. In cable-driven mechanisms, a single mechanical structure often integrates multiple one-DOF pairs to achieve complex motions. Based on these fundamental mechanism types, we define four key one-DOF motion primitives—Bend, Coil, Screw, and Compress, as shown in Fig. 6. These primitives encapsulate common motion patterns found in many cable-driven systems and serve as standardized building blocks for their design and fabrication.

We illustrate these motions on an input geometry of a rectangular cuboid with dimensions of 100mm in length ( $L = 100\text{mm}$ ), 15mm in width ( $W = 15\text{mm}$ ) augmented with cables, joints, gaps, and holes that allow for actuation using cable-driven mechanisms. Below, we detail the structure of these motion primitives and their corresponding designs for FDM 3D printing, and show they can be combined to achieve a large design space for XStrings objects. Later, in the Design Tool section, we show how these primitives can be parameterized and combined to create various different user-defined cable-driven motions.

### 4.1 Bend

The Bend Primitive, shown in Fig. 6, comprises  $n$  joints (in our example, we set  $n = 12$ ) and a single driving cable, with each pair of links allowing rotational motion between them. The rotational angle at each joint is  $\theta_i$ , which can be controlled by the size and shape of the gap between the two links. We set  $\theta_i = \frac{\theta}{n}$  so that the total bending angle about the  $x$ -axis  $\theta = \sum_{i=1}^n \theta_i$  (so in our example case,  $\theta_i = 15^\circ$ ,  $\theta = 180^\circ$ ). Then, by fixing one end of the primitive to the origin of the  $x, y, z$  axes, we can calculate the position of the endpoint of the bend primitive as:

$$(x, y, z) = \left( 0, \frac{L}{\theta} \cdot (1 - \cos \theta), \frac{L}{\theta} \cdot \sin \theta \right) \quad (1)$$

This bend primitive structure is designed using the parametric design tool Grasshopper. We started the design process by generating a single triangular prism with an internal angle of  $\theta_i$  and then duplicate them  $n$  times in a linear array. We then use these triangular prism to cut the input geometry (Boolean Difference) to create  $n$  gaps on the geometry, remaining  $n + 1$  links. We also design a compliant bridging joint that connects each link in series, enabling rotational motion through the deformation of the flexible material. Finally, using the method described in Fig. 6, holes for the cable within the links are generated to ensure that the cable can transmit force directly to the effector's endpoint, thereby driving the motion of the entire bend primitive.

### 4.2 Coil

Building on the Bend Primitive, we developed a Coil Motion Primitive, as illustrated in Fig. 6, by adjusting the angles between the primitive's segments. Unlike the Bend Primitive, the gaps in the Coil form an angle  $\phi$  with the  $y$ -axis direction of the input geometry.

This causes the movement of the Coil to no longer directly align with the direction of the  $x$ -axis when actuated, but rather results in a non-axis aligned helical coiling motion. As each segment bends by  $\theta_i$ , the overall shape coils along the  $y$ -axis (in this case, the  $y$ -axis lines up the structure's own helical axis). The primary parameters for this coil primitive include the number of turns  $N$ , radius  $r$ , and spring length  $L_s$ .

$$(x, y, z) = \left( \sqrt{L^2 - (2\pi r N)^2}, r \cdot \cos(2\pi N), r + r \cdot \sin(2\pi N) \right) \quad (2)$$

The workflow for 3D-modeling a Coil Motion Primitive is very similar to that for the Bend Primitive. We similarly use  $n$  triangle prisms to cut the input geometry. The difference is that, before cutting, triangular prisms are rotated by an angle of  $\phi$ , creating a  $(90 - \phi)$  degree angle between the gap direction and the geometry's direction. On this basis, we then add cables and joints, which serve as the driving mechanism and movable structure for the entire primitive.

### 4.3 Screw

The Screw Primitive is structured as a spring that screws around the  $z$ -axis while simultaneously shortening its length during actuation. As illustrated in Fig. 6, when the screw primitive is driven, it coincides the behavior of a spring that contracts in length when rotated around its own longitudinal axis.

The Screw Primitive consists of a continuous helical structure characterized by its length  $L$ , radius  $r$ , and extreme screw angle  $\theta$ . The screwing motion is defined by the angular displacement of the endpoint of the structure  $\theta_z$  around the  $z$ -axis, which causes the structure to compress  $\Delta z$  along its axis of rotation. As the structure screws, each incremental rotation of  $\Delta\theta_z$  causes a corresponding reduction in length, given by

$$\Delta z = L \cdot \left( 1 - \cos \left( \frac{\Delta\theta_z}{2} \right) \right) \quad (3)$$

During the screwing motion, the spring rotates around the  $z$ -axis, and its position changes accordingly. The final coordinates of the effect end after a total screw angle of  $\theta_t$  are

$$(x, y, z) = (0, 0, L - \Delta z) \quad (4)$$

In the design of the screw mechanism, we use  $n$  cuboids of length  $L_i$  to cut the input geometry so that each link is also a thin cuboid. When actuated, all the links fully align with each other. Based on this, we position four stiffer compliant joints in a circular array around the cable as the center, with a radius  $r$ . When the cable is actuated, these joints convert the force of the links moving closer together into a screwing motion, where

$$\sin \theta_i = \frac{2 \cdot L_i}{r}, \quad \theta_z = \sum_{i=1}^n \theta_i \quad (5)$$

### 4.4 Compress

The compressive structure incorporates a cable into a linear track structure. We use a basic **Prismatic pair** with one degree of freedom, allowing only sliding motion along the  $z$ -axis. By pulling the cable, two links compress along the linear track, reducing its length by  $\Delta = 0.5L$ , effectively halving its original size.

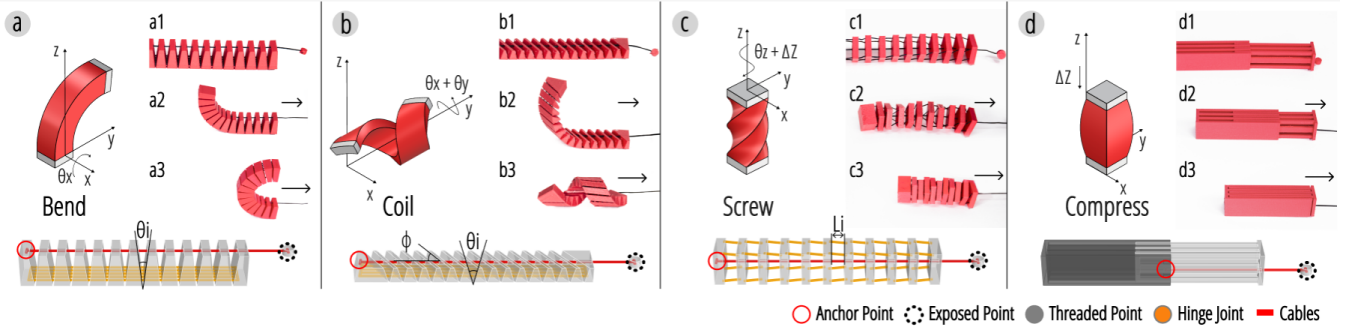


Figure 6: The four basic motion primitives of Xstrings: Bend, Coil, Screw and Compress.

## 5 DESIGN SPACE

### 5.1 Dimensional Combination of Primitives

By combining these primitives in series or parallel, we can create complex, adaptive 3D-printed structures tailored to specific functional requirements, demonstrating the versatility and potential of cable-driven mechanisms in soft robotics and advanced manufacturing.

#### Series Combination

In a series combination, multiple primitives are connected in a sequential manner and driven by a single cable. Cable actuation begins from the farthest end of the mechanism and propagates toward the base, causing cascading deformation along the sequence.

The advantage of the series combination lies in its ability to achieve complex, coordinated movements with minimal control input. Since only one cable is required to drive all connected primitives, the design of sequential mechanisms is more straightforward and compact than that of parallel mechanisms. This approach is ideal for applications requiring sequential motion of segments of an object, including robotic arms, tentacle-like structures, or bio-inspired soft robots where precise control over motion propagation is necessary (an example of this is given in Section 7.3).

Mathematically, the total driving force and deformation in a series can be mathematically represented as

$$F_{\text{total}} = F_i + \sum_{i=1}^{n-1} F_{C,\text{resistance}}, \quad \Delta L_{\text{total}} = \sum_{i=1}^n \Delta L_i \quad (6)$$

where  $\Delta L_i$  is the displacement of the  $i$ -th primitive along the  $x$ ,  $y$ , and  $z$  axes, respectively.

An example of a series mechanism is shown in Fig. 7(a). We combine seven bend primitives in series to form a long strip-shaped object, where each bend primitive is capable of bending 90 degrees and can bend in different directions. All these primitives are then controlled by a single cable. As shown in Fig. 7b, c and d, by pulling the cable, this long strip-shaped object will eventually form a square.

#### Parallel Combination

In a parallel combination, the main cable splits into multiple sub-cables, each connected to a different primitive, but all driven synchronously by a single “central” actuator. This design allows multiple sections of the mechanism to move simultaneously, providing synchronized actuation across all primitives.

The advantage of the parallel combination lies in its ability to achieve simultaneous, coordinated movements, enabling faster and more responsive actuation. This method is ideal for applications that require uniform or synchronized deformations, such as multi-fingered grippers, adaptive surface actuators, or morphing structures.

The synchronization of the sub-cables can be controlled by a central axis, and the relationship between the driving force and the actuation can be mathematically represented as

$$F_{\text{total}} = \sum_{j=1}^m F_j, \quad \Delta L_{\text{total}} = \Delta L_j \quad (7)$$

where  $F_{\text{total}}$  is the total force applied by the main cable,  $F_j$  is the force transmitted through each sub-cable, and  $\Delta L_j$  is the deformation length of the  $j$ -th primitive.

We demonstrate a parallel combination in Fig. 7(b). We create a gripper object that consists of a handle with five bending structures forming a star shape at the end. Each of the bending structures is controlled by a different cable, and these five cables are connected in parallel. This means that controlling the final single joining cable can cause all five bending structures to deform simultaneously. As shown in Fig. 7b1, b2 and b3, when this joined parallel cable is pulled by hand, all five bending structures move simultaneously.

### 5.2 Hole Placement and Joint Design

When determining the placement of threaded points and cables relative to the joints in a structure, their effect on system stiffness must be considered. If the threaded points are placed close to the joints, the moment arm is shorter, requiring greater force to generate the same torque, thereby increasing system stiffness. Conversely, positioning the threaded points farther from the joints reduces stiffness.

**Anchor Point Placement:** The placement of anchor points influences system stiffness by altering the moment arm length. A shorter moment arm requires greater force to achieve the same

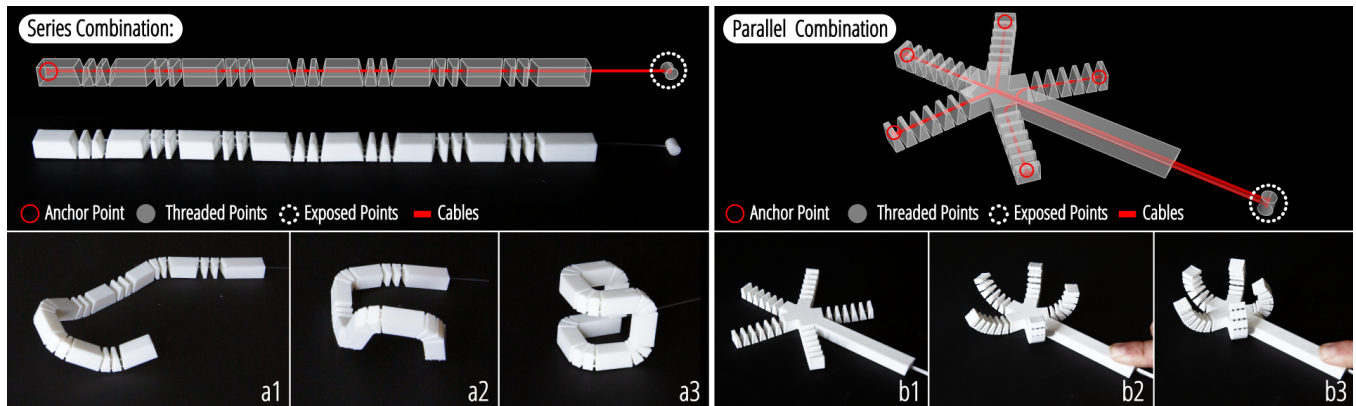


**Figure 7: (a) A series sample designed with 7 Bend primitives, forming a cube frame when actuated; (b) A paralleled sample designed with 7 Bend primitives, forming a cube frame when actuated.**

deformation, increasing stiffness, while a longer moment arm decreases stiffness. Assuming a force  $F_c$  applied at the end effector, a total structure length  $L$ , and a hole-to-hinge distance  $d$ , stiffness  $k$  follows the relationship:

$$k = \frac{F_c}{\delta y}, \quad \delta y \propto d$$

where  $\delta y$  represents vertical deformation at the endpoint. Thus, stiffness decreases as  $d$  increases, meaning that placing holes farther from the joints reduces system stiffness.

**Joint Design:** The stiffness of joints is determined by the spring constant  $k_i$ . Since the joints are in series, their equivalent stiffness  $k_{\text{joints}}$  is given by:

$$\frac{1}{k_{\text{joints}}} = \sum_{i=1}^n \frac{1}{k_i}$$

Higher joint stiffness contributes to greater overall system stiffness, making it crucial to optimize joint material and structure according to design requirements.

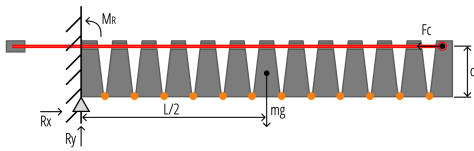


**Figure 8: Illustration of the Xstrings system and mechanical setup.**

The joint type determines  $k_n$  and affects the total joint stiffness,  $k_{\text{joints}}$ . **Elastic joints** provide high stiffness with nonlinear deformation under strain, enabling energy recovery after actuation. **Compliant joints** offer moderate stiffness and predictable deformation, ideal for lightweight, compact mechanisms. When composed of multiple small bridges in parallel, the joint stiffness equals the sum of the bridges' stiffness. **Mechanical joints** contribute the lowest stiffness.

**Threading Hole Geometry:** Threading hole geometry minimally affects stiffness if the hole diameter exceeds the cable diameter. Smaller holes shift  $F_c$  from a point force at the end effector to a distributed force along the structure, altering bending dynamics and compromising the mechanism. Optimizing hole geometry ensures smooth cable sliding and consistent force transmission (see Section 8.4).

### 5.3 Cable Shapes

Compared to traditional cable-driven mechanisms, the customization capabilities of 3D printing allow for the fabrication of cables with various shapes, offering greater design flexibility. In Fig. 9, we present two distinct cable shapes designed to provide haptic feedback and motion control, respectively.

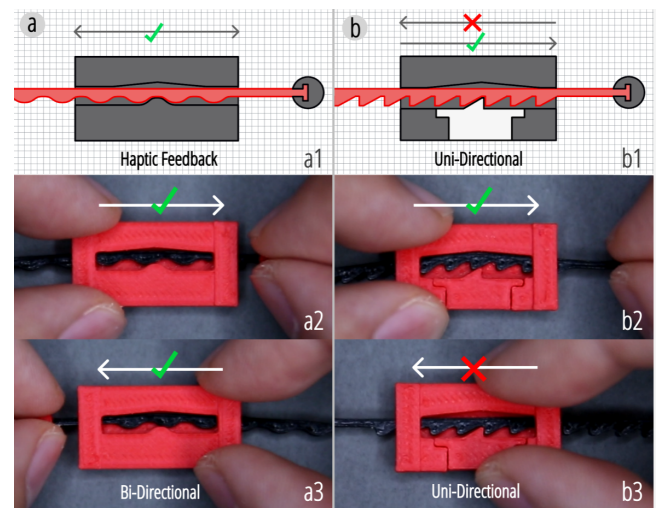


**Figure 9: Two distinct cable shapes designed to provide haptic feedback and motion control**

The cable in Fig. 9a is designed in a wave-like shape. As it passes through a component's hole, each peak of the wave collides with the



underneath bump inside the hole, which perform a haptic feedback. This design provides a segmented tactile sensation during pulling, enabling users to perceive the distance of the cable actuation.

Inspired by the design principles of zip ties, Fig. 9b features sharper angles at the bends. When pulled and engaged with the underneath ratchet teeth, the cable interlocks with them, preventing reverse movement. The lock can be released by moving the white component downward, allowing for a uni-directional mechanism that can mimic complex motions, such as a snake coiling or a hand grasping. The potential design opportunities enabled by such a uni-directional motion mechanism are explored in greater detail in Section 7.4.

## 5.4 Embedded-Cable Actuation

In our regular cable-driven mechanism design, objects are actuated by pulling on or manipulating the exposed ends of the cables. However, Xstrings' integrated printing technology enables actuation methods that do not require direct manipulation of the cable endings. We refer to this actuation technique as embedded-cable actuation.

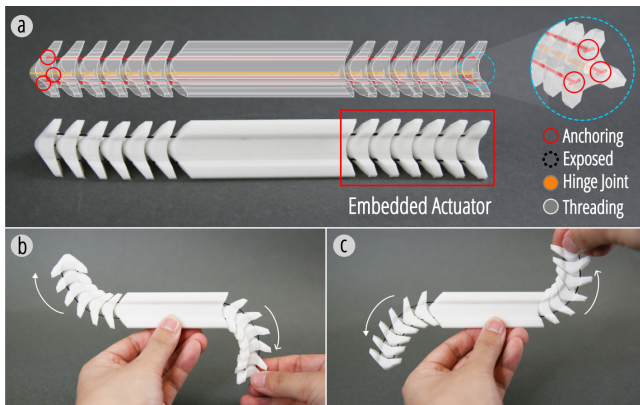


**Figure 10: A sample of a 3D-printed spine with embedded cable actuation, where one of the ends of the spine moves when the opposite end is actuated.**

As shown in Fig. 10, the structure contains two segments of spinal-like structures on the left and right, each embedded with three cables and hinge joints, forming an interlinked mechanism. When the middle section is fixed in place, any deformation applied to the tail end results in an opposite deformation at the head end (Fig.10b and c), and vice versa. When the cable ends are exposed, manually controlling the three cables separately to direct the head in a specific direction or perform complex movements, such as swinging or looking around, is quite counterintuitive. The structure design enabled by Xstrings adds possibilities for more natural methods of interaction with multi-axis cable-driven mechanisms and provides a more efficient manufacturing approach for cable-driven embedded interlinked mechanisms. We will illustrate the use of this technique in an application in 7.4.

## 6 DESIGN TOOL

Xstrings software uses Rhinoceros 8 as the design environment and Grasshopper as both a computational tool and an intermediary user interface. In broad terms, the user workflow is as follows: input a geometry for embedding cable-driven mechanism; select desired primitives and define the number of segments and specify the angle after deformation; set a curve as input of cable and tune the cable width and shape of end; export and preview the results and generate the printing file.

### 6.1 User Workflow

**Embedding Primitives:** After inputting a geometry drawn in the Rhinoceros environment, users can select a primitive from our library (as shown in Fig. 11). The main interface will display the currently edited segment (shown in red) and the other segments (shown in blue). By adjusting the sliders in the interface, users can edit the bending degree and the number of segments of the actuated shape. We provide some pre-tested initial values as references to help users achieve some of our primitive examples. Once users have implemented a primitive in a specific segment, they can add new segments to achieve other primitives. In Fig. 11, the tip of the tentacle is designed as a coil primitive, while the body is designed with bend primitives to both left and right, respectively.

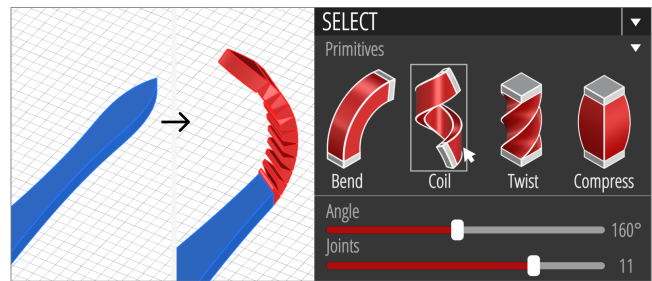


**Figure 11: Primitives Embedding process in Xstrings system.**

**Modifying the Cable:** In this step, users can specify the parameters for each cable, including its shape, width, and thickness, based on the estimated maximum force exerted by the objects. The Xstrings system will then automatically generate a T-shaped anchor point to attach the cable to the furthest end of the end effector. For the threaded points, the design tool offsets the cable's surface by 0.5mm and uses a Boolean difference to create holes for all threaded components. This parametric modeling process maintains a 0.5mm distance between the cable and the wall of the hole, reducing friction while still providing enough control over the cable's path during manipulation. For the exposed points, we offer three types of shapes: (1) Dot and (2) Ring, which are designed for manual manipulation; and (3) Spool, which can be directly connected to a servos and controlled electrically.

**Printing Settings for different parts:** To increase compatibility and enable the integration of cable-driven mechanisms on any multi-material 3D printer, we opted not to generate G-code for a specific printer model. Instead, we provide parameter settings for

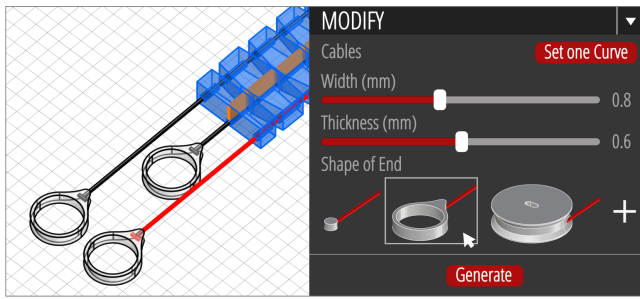


Figure 12: Cable Modifying in Xstrings system.

different slicing software. We have successfully implemented this functionality on three types of printers: Ultimaker S5, Ultimaker 3, and Bambu X1. The output files will include three separate files: Main (PLA), Cable1 (Nylon), and Cable2 (Nylon). In our example, “Main” represents the main body of the tentacle, “Cable1” is the first layer of all cables, and “Cable2” represents the remaining layers of the cables. Using the Ultimaker S5 settings as an example, the “Main” part is printed with the settings recommended by the PLA material supplier; “Cable1” is printed at 90% flow rate, 20mm/s regular speed, and 40mm/s bridge wall speed; “Cable2” is printed at 20mm/s speed with a 110% flow rate. (Parameters for other FDM 3D printer are provided in the appendix.) After slicing and exporting the files, the print can be completed. The manipulation scenarios are shown in Fig. 14.

## 6.2 Inverse Design

Beyond embedding basic primitives, Xstrings can manipulate elongated blocks into arbitrary 2D curves. In cable-driven robotics, achieving complex curve motions often requires multi-segment control systems, involving multiple motors and cable drive mechanisms connected to various positions [35, 56].

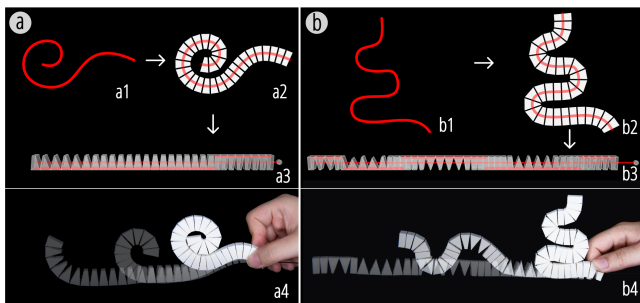


Figure 13: Inverse design resulting from two different input curves: (a) a spiral shape, and (b) a serpentine shape.

These systems are often large and require complex, labor-intensive assembly processes. To simplify this, Xstrings introduces an automated cable-driven mechanism design tool that enables users to intuitively design such mechanisms using predefined primitives. Our approach abstracts away the complexities of designing individual

surface geometry features—such as holes and joints—by generating them automatically. This allows the entire mechanism to be 3D printed in a single step, streamlining the fabrication process.

To abstract away the tedious low-level details of cable-driven mechanism design, we developed an automatic inverse design algorithm that transforms user-input curves into segmented polylines to define the shape of their structure. We do this by replacing each polyline with a series of blocks that are unfolded into straight strip, as illustrated in Fig. 13, and connected with cables and hinge joints.

We use our inverse algorithm to automatically determine the positions of the joints, the gap sizes and the angles. This process ensures that the resulting driven shape and curvature match the user’s input precisely. Fig. 13 shows two such printed strips generated from user-defined input curves that are then converted into segmented strips and laid out flat, such that when actuated they deform back into the shape of the original input curve.

## 7 APPLICATIONS

### 7.1 Multi-Directional Tentacle Actuation

As mentioned in the previous section, we utilized the design tool to fabricate a controllable tentacle, which consists of 28 components and is printed at the maximum diagonal length (352 mm) of the 3D printing platform. This mechanism incorporates three cables that control the structure to bend left, coil at the tip, and bend right, respectively (as shown in Fig. 14 b1, b2, and b3).

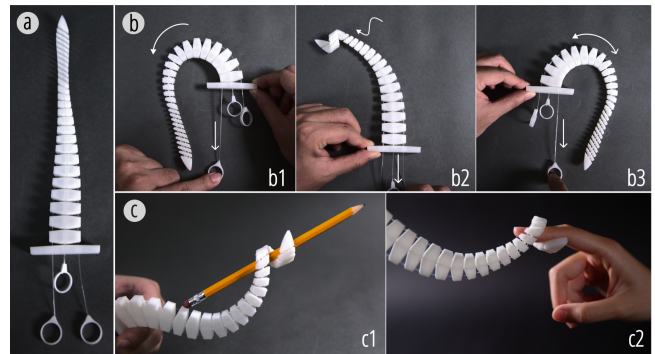


Figure 14: (a) A one-step-printed Xstrings tentacle in its initial position. (b) Controlled movements showing the tentacle’s ability to perform bend and coil motions through different cable manipulation. (c) Application scenarios of the tentacle manipulating and grasping objects.

Due to the real-time responsiveness and accuracy of cable-driven tip control, the tip’s coiling action enables better interaction with objects, such as grasping a pencil and wrapping a finger. The design of linked joints allows for precise control of the tip’s spatial position, helping it to locate and drag objects more accurately. This case demonstrates how Xstrings utilizes cable-driven mechanisms in 3D-printed dynamic structure to achieve complex motions, providing next-level control and interactivity for FDM 3D printing.



## 7.2 Bio-Inspired Lizard Robot

In tasks such as exploring unknown areas, environmental modeling, and emergency assistance [5, 11], multiple robots can work collaboratively to quickly accomplish complex operations. However, most current bio-inspired crawling robots, while having significant advantages in traversing complex and diverse terrains [60], are limited in their widespread application and mass production due to high manufacturing costs and complex production processes.

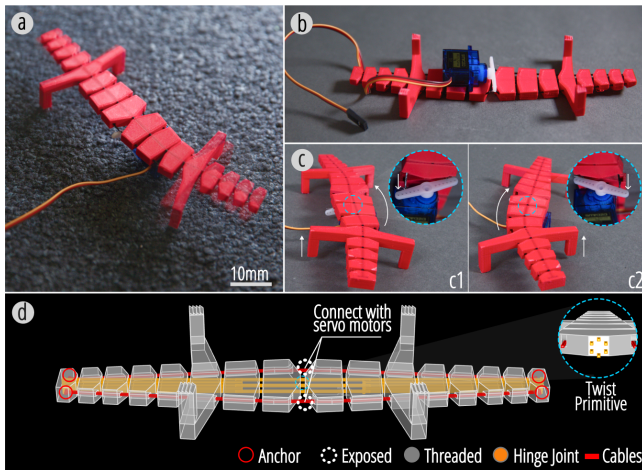


**Figure 15: (a) A print-in-place Xstrings lizard robot with biomimetic locomotion. (b) The robot connected to a Micro Servo Motor (SG90 9G). (c1-c2) Snapshots of the robot's motion showing its body bending and screwing. (d) The structural diagram with screw and bend primitives.**

To address this issue, we propose a low-cost bio-inspired lizard robot design based on the Xstrings cable-driven mechanism, as shown in Fig. 15. This robot can be actuated electronically to mimic natural locomotion by alternately bending its body left and right while lifting its back legs. Such movements create a shuffling motion that utilizes surface friction and shifts the center of mass, propelling the robot forward. The precise cable actuation enables the robot to navigate narrow spaces and various terrains effectively. This approach, using a print-in-place manufacturing method and economical components—costing only \$1.90 for the motor and \$0.40 for the printing material, provides a possible solution for mass production of cable-driven mechanism.

## 7.3 Fashion and Art Design

3D printing has been widely embraced by artists for sculptures, clothing, jewelry, and other fashion pieces. Herschel Shapiro's static wall sculptures, known for their repetitive and varied designs, have garnered significant attention [49]. Xstrings extends these artistic possibilities by introducing assembly-free, cable-driven movable structures.

Using Xstrings, we designed and fabricated a dynamic wing-shaped sculpture (Fig. 16) that features seven parallel arrays of eight curved plumes. These plumes are driven by a single cable actuating eight bending primitives via a rotating disk. When the

disk rotates, the plumes rise from flat to upright, evoking imagery of porcupine spines or bird feathers. Printed with dual-color Silk PLA Filament, the plumes transition from blue to purple as they move, showcasing Xstrings' potential for creating interactive, visually striking art. Beyond art, such structures could also be applied in scenarios like MetaReality [7], where they enable customizable and dynamic haptic feedback for VR/AR environments. Our approach offers similar potential for the advancement of physical interfaces, providing a rapid single-step 3D printing method that eliminates the need for manual assembly and enhances the user experience.

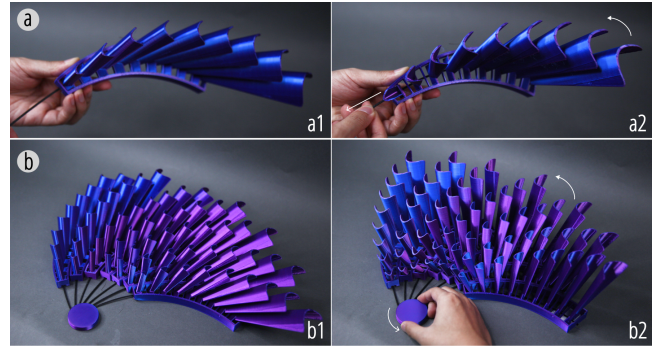


**Figure 16: An Xstrings dynamic sculpture, actuated with a rotatable disk.**

## 7.4 Claw with Embedded Actuation

We designed a cable-driven bird claw with an embedded actuation mechanism to fully explore the Xstrings design and fabrication space. This design integrates the actuator into the claw's elbow for an ultra-lightweight design, converting forces into gripping motions—ideal for aerial applications.

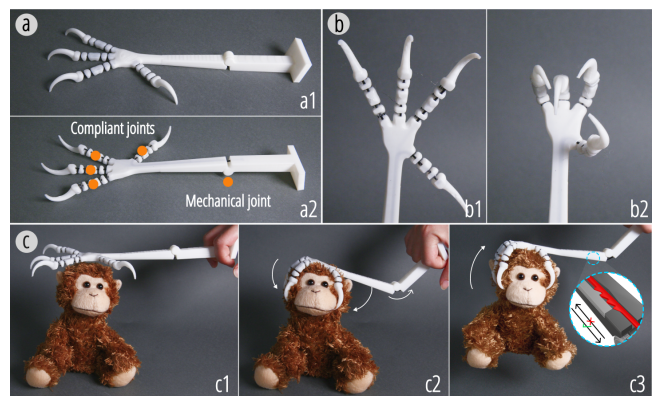


**Figure 17: (a) An Xstrings claw, featuring four fingers with compliant joints and an elbow with a mechanical joint. (b) Display of the claw fingers in open and closed positions. (c) The operation of the claw grasping an object by bending the elbow to drive the cable. Due to the ratchet design of the cable, the claw does not release during this process.**

In specific, this print-in-place structure consists of four fingers, each composed of five series of bending primitives connected by compliant joints. The four fingers are arranged in a parallel configuration and actuated by a single cable. In addition, there is a mechanical joint lower in the arm of the claw, allowing the elbow of the structure to bend. This is a fully embedded, self-contained mechanism (as described in Section 5.3), so instead of the user or a motor directly engaging with the exposed cable, the bending of the elbow itself pulls on the cable, causing the claw to grip. This design allows the user to pick up and transport objects by applying a single force to the elbow of the arm. Due to the ratchet design of the cable shape (Section 9), the bird claw only tightens and does not release during this process, ultimately achieving a firm grip on the object.

## 8 EVALUATION

### 8.1 Deriving the Displacement Relation Between Cable Draw and End Effector

In this section, we evaluate the relationship between the cable draw and end effector position of Xstrings objects for each of the bend, coil, screw and compress primitives. To characterize the behavior of each primitive, we use an experimental setup that measures how the endpoint of an Xstrings object moves as we pull the cable by a given distance.

We define the origin of our coordinate system to be at location where the exposed end of the cable leaves the Xstrings structure, denoted as  $(0, 0, 0)$ . The starting position of the end effector is denoted as  $(100, 0, 0)$ .

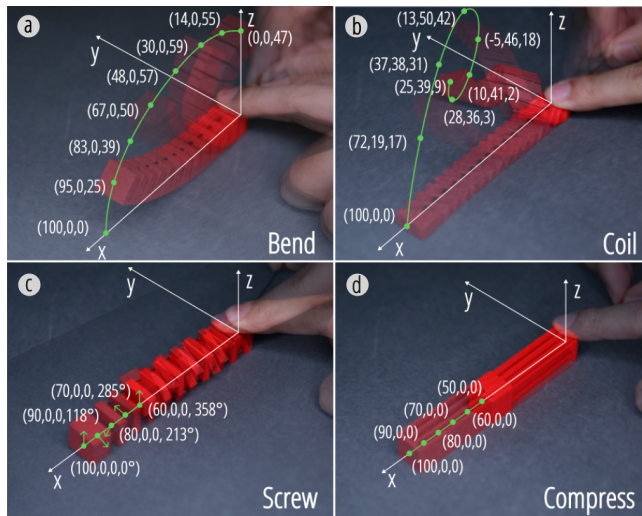


**Figure 18: Relationships between cable draw displacement and end effector displacement.**

To perform a single measurement, we pull the cable by our increment distance  $\Delta d$ . We then fix the cable's endpoint and record the  $x, y, z$  coordinate of the end effector of the Xstrings primitive, denoted as  $C_n$ . After this we pull the cable by an additional  $\Delta d$  and repeat. This process is repeated for a total of  $N$  steps, with the total

pulling length denoted as  $D$ . The relationship can be expressed formally as

$$\begin{cases} D = N \cdot \Delta d, \\ C_n = f(n \cdot \Delta d), \quad n = 1, 2, \dots, N. \end{cases} \quad (8)$$

Using this method, we recorded the paths of the end effector for four samples in the three-dimensional coordinate system, shown in Fig. 18. Below, we discuss the results of this experiment for each primitive.

**Bend:** We conducted experiments on the bend primitive with  $\Delta d = 0.5$  mm and  $D = 3.46$  mm. The end effector trajectory exhibited nonlinear behavior, with displacement amplitude decreasing as the cable retracted, eventually reaching a limit position. For example, when  $n = 1$ , the displacement from  $y_0$  to  $y_1$  was 25.5 mm, but at  $n = 6$ , the displacement from  $y_6$  to  $y_7$  decreased to 16.5 mm. Deformation was non-uniform, with the first seven joints near the end effector bending more significantly, while the remaining six joints remained stationary. This behavior arises from cumulative gravitational forces and the elasticity of the compliant joints.

**Coil:** We conducted experiments on the coil primitive with  $\Delta d = 0.5$  mm and  $D = 3.34$  mm, the motion was nonlinear and non-uniform, similar to the bend primitive. For  $n = 0$  to 4, the coil transitioned into a near-helical shape with a larger radius, then tightened gradually for  $n = 4$  to 7. This tightening demonstrates its use as a strip-like gripper, leveraging its gradual contraction for gripping functionality.

**Screw:** In the test of the screw primitive with  $\Delta d = 1$  mm and  $D = 4$  mm, the end effector's motion involved rotation about the  $x$ -axis. To capture this, we recorded an additional parameter  $\theta$ , the rotation angle of the endpoint. The end-effector trajectory was nonlinear, where the amount of angular rotation of the system decreased for larger  $n$ , though the decrease was less than the theoretical value due to joint flexibility. From  $n = 0$  to  $n = 3$ , joint bending partially offset the rotation, while between  $n = 4$  and  $n = 5$ , reduced gaps between blocks lessened the bending effect. Ultimately,  $\theta$  reached  $358^\circ$ , closely matching the design target.

**Compress:** For the compress primitive, composed entirely of mechanical sliding pairs, we used  $\Delta d = 1$  mm and  $D = 5$  mm. As expected, the relationship between  $y_n$  and  $n \cdot \Delta d$  exhibited a perfectly linear correspondence.

### 8.2 Comparison of the Time Efficiency of Xstrings with Manual Assembly

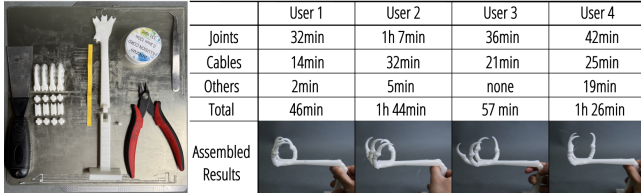
To evaluate the efficiency of our approach, we compare the time taken to produce all-in-one printed objects with printed-assembled counterparts. Using the claw gripper model (Section 7.4), we divided it into 19 parts for 3D printing and provided participants with an assembly toolkit (Fig. 19).

The study involved 4 participants (2 males, 2 females) with varying levels of experience: User 1 had extensive knowledge of 3D printing assembly and cable-driven robotics; Users 2 and 3 had general assembly experience but no familiarity with cable-driven models; User 4 had minimal prior experience assembling manual objects.

The manual assembly process included the following steps:



- Participants received a tutorial and demonstration, including instructions for installing pivots, threading cables, and tying knots, with a completed sample for reference.
- Assembly times for joints and cable threading/tightening were recorded.
- Assistance from staff, if requested, was logged as “other” time.



	User 1	User 2	User 3	User 4
Joints	32min	1h 7min	36min	42min
Cables	14min	32min	21min	25min
Others	2min	5min	none	19min
Total	46min	1h 44min	57 min	1h 26min

**Figure 19: Time taken for the manual assembly of claw grippers and the resulting assembled objects.**

**Results and Discussion:** The time analysis revealed that the conventional print-assembly approach required **1h 25min** for 3D printing and an average of **1h 13min** for assembly. In contrast, the Xstrings method required **1h 36min** for printing but eliminated assembly entirely, saving 1 hour and 11 minutes, approximately 40% of the total time.

During the manual assembly process, common issues included: improperly sized holes for metal pivots (Users 1, 2, 4), difficulty threading cables through the thumb’s channel (Users 2, 4), and knots that frequently loosened (User 4). Additionally, User 2 faced challenges grasping small joint nodes due to larger fingers, leading to delays.

The manually assembled models exhibited varied grasping postures due to inconsistencies in knot placement and cable tension, resulting in uneven grasping tightness (Users 3, 4) and poor finger synchronization (Users 2, 3). Furthermore, the toolkit cables lacked flexibility for implementing uni-directional grasping mechanisms.

In summary, the Xstrings method significantly enhances time efficiency by eliminating manual assembly, reducing the overall time required compared to the conventional print-assembly approach. It also addresses issues of accuracy and consistency, mitigating the impact of human error on the final product.

### 8.3 Assessing Cable Properties through 3D Printing Parameter Tuning

To gain a comprehensive understanding of the influence of print temperature and speed on the quality of embedded cables in 3D printing, we conducted a series of controlled experiments to identify the optimal parameters for producing high-quality cable embeddings. All evaluations were conducted using printed samples, each consisting of three printed cables with a width of 0.8 mm and a height of 0.6 mm. These cables were subjected to different combinations of print temperatures and speeds. Print temperatures were set at 240°C, 260°C, and 280°C, while print speeds varied from 10 mm/s to 30 mm/s. The resulting cable quality, shown in Fig. 20, was categorized into three levels: “Failed,” “Defective,” and “Optimal,” based on visual inspection and the integrity of the embedded cables.

**Print Temperature:** Print temperature plays a crucial role in determining the quality of the embedded cables. At a lower temperature of 240°C, the quality of the cables ranged from “Defective” at lower speeds (10 mm/s and 15 mm/s) to “Failed” at higher speeds (20 mm/s to 30 mm/s). The optimal print temperature for achieving high-quality cables was found to be 260°C. At this temperature, the embedded cables demonstrated “Optimal” quality at print speeds of 10 mm/s to 20 mm/s. However, as the speed increased to 25 mm/s, the quality decreased to “Defective,” and at 30 mm/s, it resulted in “Failed” prints. At a higher temperature of 280°C, the quality was generally poor, with “Defective” observed at speeds of 10 mm/s and 15 mm/s, and “Failed” quality at speeds of 20 mm/s and above.

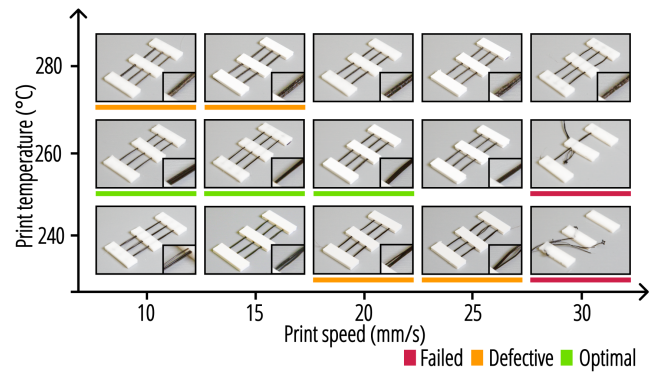


**Figure 20: Results of cable prints with different printing parameters.**

**Print Speed:** The print speed also significantly affects cable quality. Lower print speeds, specifically 10 mm/s and 15 mm/s, yielded better results across different temperatures, particularly at 260°C where the cable quality was “Optimal.” However, as the speed increased to 20 mm/s, the prints remained “Optimal” at 260°C but were “Defective” at other temperatures. Speeds of 25 mm/s and 30 mm/s consistently produced “Defective” or “Failed” prints across all temperature settings, indicating that higher print speeds adversely impact the quality of the embedded cables.

Through our technical analysis, we found that the optimal combination for high-quality cable embedding is a print temperature of 260°C combined with a print speed between 10 mm/s and 20 mm/s. Print speeds exceeding 15 mm/s, especially at temperatures lower than 260°C or higher than 280°C, tend to result in lower quality or failed prints.

### 8.4 Exploring the Tension Limits of Cables and Systematic Stiffness

In this experiment, samples were fabricated using a combination of Nylon and Polylactic Acid (PLA) materials through 3D printing. Nylon serves as the cable, anchored at both ends within the PLA. For each width, shown in Fig. 21, five samples were printed and tested five times, with the resulting curves representing the average of these experiments.

**Mathematical Model:** In our 3D printing setup, the minimum printing path for the filament is  $w_i = 0.4$  mm, and so the width of

the filament is  $w = n \times w_i$ , where  $n$  is an integer. When  $n$  is even, the filament is formed by two passes of 3D printing, resulting in a more uniform mass distribution, and the break usually occurs in the middle of the filament. When  $n$  is odd, the filament is more likely to break closer to one of the endpoints due to uneven mass distribution.

To understand the influence of width on the tensile force limit, we assume the cross-section of the filament is rectangular. The cross-sectional area  $A$  can be represented as the product of the filament width  $w$  and thickness  $t$ , with the proportional tensile force limit  $F_c$  is:

$$\begin{cases} F_c \propto k_c = \frac{EA}{L}, \\ A = w \cdot t. \end{cases} \quad (9)$$

This formula indicates that as the filament width increases, the cross-sectional area also increases, allowing the filament to withstand greater tensile forces.

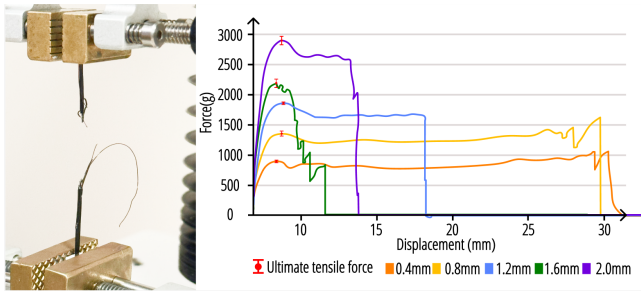


Figure 21: Ultimate tensile force of cables with different width from 0.4 mm to 2 mm.

**Effect of Width on Tensile Force Limit:** Experimental results indicate that increasing filament width significantly enhances the tensile force limit. For instance, a 2.0 mm filament withstands 2800g (purple curve), while a 0.4 mm filament withstands 800g (orange curve), illustrating the influence of cross-sectional area on tensile strength. When  $n$  is even, filaments typically break at the center, while odd  $n$  results in failure near endpoints, highlighting the impact of printing path and material distribution on tensile properties.

### 8.5 Fusion Test Between Different Materials

In this experiment, we evaluated the fusion capability between six common 3D printing materials. Generally, better fusion capability indicates that, in multi-material 3D printing, the materials are less likely to separate from each other. Some multi-material 3D printing studies attempt to enhance fusion capability to increase the strength of multi-material components [2]. In contrast, we aim to identify two materials with poor fusion capability to enable the printing of movable threaded points in Xstrings.

Six common 3D printing materials were selected: Nylon, PC, TPU, ABS, PETG, and PLA. Using CURA’s default settings, multi-material samples were printed, pairing each material with another. Each 2mm-high sample consisted of 1mm of the first material and 1mm of the second. After cooling, attempts were made to separate the materials, with results categorized as: natural separation,

Table 1: Fusion test result of every two materials.

	PLA	Nylon	PC	TPU	ABS	PETG
PLA						
Nylon	Green					
PC	Orange	Green				
TPU	Orange	Orange	Red			
ABS	Red	Orange	Red	Red		
PETG	Red	Orange	Red	Red	Red	

Legend: Green Naturally Detach, Orange Manually Separate, Red Inseparable

manual separation, or inseparable (breaking within one material). Results show that PLA-Nylon and PC-Nylon pairs naturally separate, making them ideal for threading points of Xstrings.

### 8.6 Fatigue Limits Test of Cables

We used a 28BYJ-48 Step Motor to conduct a fatigue limits test on the Xstring. The servo’s stepping parameter is set to 540 (out of 2048 per full revolution). In other words, we actuate a driving rod to pull the cable along an arc of 90 degrees. The speed parameter is set to 15 revolutions per minute, with each loop taking a total of 10 seconds: 4 seconds upward, 1 second pause, 4 seconds downward, and another 1 second pause. The experiment lasted for a total of 7 days and 8 hours, with over 60,000 cycles, eventually breaking at the connection point between the cable and the driving rod.

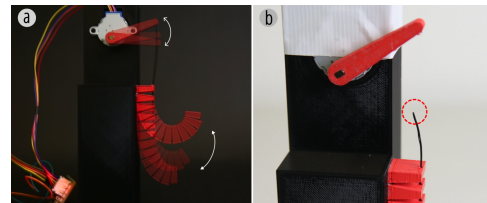


Figure 22: Fatigue limits test scenario and final breaking points.

## 9 LIMITATIONS AND FUTURE WORK

We next address the limitations within our work and explore potential directions for future research.

### 9.1 Compatibility of Xstrings with Manual Modifications and Iterations

Xstrings provides an end-to-end manufacturing solution for cable-driven mechanisms while supporting manual adjustments and repairs during prototyping. Such interventions align with user intuition, fostering creativity and enabling design exploration.

The thermoplastic properties of PLA facilitate modifications. For example, as shown in Fig. 23, a damaged cable in a tentacle prototype was repaired by melting PLA with a soldering iron to create a knot-compatible hole, adding a new knotting point 2 mm from the original loop. These adjustments kept the prototype functional, avoiding waste. Users can also close holes, reshape surfaces, or add metallic components, enhancing versatility.

Xstrings enables efficient manufacturing while allowing users to repair and adjust prototypes, extending their lifespan, improving sustainability, and encouraging creative iteration.

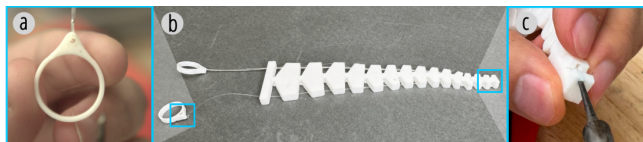


**Figure 23: One of a prototype’s cable is replaced with fishing string by manual tinkering.**

## 9.2 Only Flat-planar Cables

Despite Xstrings’ significant advancements in the automated integration of cable-driven mechanisms into 3D objects, our current approach is limited by the constraints of 3D printing technology. Specifically, the cables in Xstrings can only be printed on the  $(x, y)$ -plane. This limitation stems from the extrusion process of FDM 3D printers, where cables need to be printed layer by layer. Stacking material along the  $z$ -axis makes the cable very fragile due to the inadequate interlayer bonding strength of nylon, which is insufficient to withstand repeated tensile forces. Thus, printing high-performance cable materials in three-dimensional space becomes challenging.

As a result, our current approach restricts cable paths to the printing plane to ensure the stability and precision of embedded cable-driven mechanisms. Although the cable layout is planar, the actuated objects can still move in multiple dimensions. Future work could explore advanced multi-axis 3D printing techniques or customized G-code manufacturing methods to overcome this limitation, enabling more diverse and spatially complex cable-driven mechanisms.

## 9.3 Generalizability to Other FDM Printers

The extent to which Xstrings results can be directly applied to other users’ set-ups is conditional on the selection of printing material and printer model. Our evaluation establishes explicit parameter mapping to our 3D printer (Ultimaker and Bambu) and material choice (Nylon 66, xypolyer). Users may need to perform some calibration steps to precisely align the printing parameters of their specific fabrication set-up to Xstrings’s mechanical properties.

## 10 CONCLUSION

We present Xstrings, a novel approach to 3D printing cable-driven mechanisms, which integrates cable-driven systems directly into the geometry of 3D-printed objects, simplifying their fabrication process. Unlike traditional methods that require labor-intensive manual assembly, Xstrings automates the design and fabrication, supporting four types of cable-driven interactions—bend, twist, coil, and compress—using dual-material FDM 3D printing. It enables rapid prototyping and the production of complex dynamic structures without the need for additional assembly.

Xstrings demonstrates its versatility through various applications, such as dynamic fashion accessories, bionic robots, and adaptive prototypes. The technical evaluations we present highlight the effectiveness of different printing parameters in optimizing the mechanical properties of the embedded cables, addressing challenges related to tensile strain, repeatability, and material fusion. The design tool we developed as part of this method facilitates user-friendly integration of cable-driven mechanisms, allowing for customizable designs suited to a wide range of practical applications.

Overall, Xstrings presents a significant advancement in personal fabrication and robotics, offering a low-cost, efficient, and scalable solution for creating dynamic 3D-printed objects with integrated motion capabilities.

## REFERENCES

- [1] Cemil Bagci. 1971. Degrees of Freedom of Motion in Mechanisms. (1971).
- [2] E Brancewicz-Steinmetz, R Valverde Vergara, VH Buzalski, and J Sawicki. 2022. Study of the Adhesion Between TPU and PLA in Multi-material 3D Printing. *Journal of Achievements in Materials and Manufacturing Engineering* 115, 2 (2022).
- [3] Xiang ‘Anthony’ Chen, Stelian Coros, and Scott E. Hudson. 2018. Medley: A Library of Embeddables to Explore Rich Material Properties for 3D Printed Objects. In *Proceedings of the 2018 CHI Conference on Human Factors in Computing Systems* (Montreal QC, Canada) (CHI ’18). Association for Computing Machinery, New York, NY, USA, 1–12. <https://doi.org/10.1145/3173574.3173736>
- [4] Jacinto Colan, Ana Davila, Yaonan Zhu, Tadayoshi Aoyama, and Yasuhisa Hasegawa. 2023. OpenRST: An Open Platform for Customizable 3D Printed Cable-Driven Robotic Surgical Tools. *IEEE Access* 11 (2023), 6092–6105. <https://doi.org/10.1109/ACCESS.2023.3236821>
- [5] Micael S. Couceiro, David Portugal, and Rui P. Rocha. 2013. A Collective Robotic Architecture in Search and Rescue Scenarios. In *Proceedings of the 28th Annual ACM Symposium on Applied Computing* (Coimbra, Portugal) (SAC ’13). Association for Computing Machinery, New York, NY, USA, 64–69. <https://doi.org/10.1145/2480362.2480377>
- [6] Ashley Del Valle, Mert Toka, Alejandro Aponte, and Jennifer Jacobs. 2023. PunchPrint: Creating Composite Fiber-Filament Craft Artifacts by Integrating Punch Needle Embroidery and 3D Printing. In *Proceedings of the 2023 CHI Conference on Human Factors in Computing Systems* (CHI ’23). Association for Computing Machinery, New York, NY, USA, Article 216, 15 pages. <https://doi.org/10.1145/3544548.3581298>
- [7] Martin Feick, Donald Degraen, Fabian Hupperich, and Antonio Krüger. 2023. Metareality: enhancing tactile experiences using actuated 3D-printed metamaterials in virtual reality. *Frontiers in Virtual Reality* 4 (2023), 1172381.
- [8] Shuyue Feng, Cheng Yao, Weijia Lin, Jiayu Yao, Chao Zhang, Zhongyu Jia, Lijuan Liu, Masulani Bokola, Hangyue Chen, Fangtian Ying, et al. 2023. MechCircuit: Augmenting Laser-Cut Objects with Integrated Electronics, Mechanical Structures and Magnets. In *Proceedings of the 2023 CHI Conference on Human Factors in Computing Systems*. 1–15.
- [9] Evgueni T Filipov, Tomohiro Tachi, and Glaucio H Paulino. 2015. Origami Tubes Assembled into Stiff, Yet Reconfigurable Structures and Metamaterials. *Proceedings of the National Academy of Sciences* 112, 40 (2015), 12321–12326.
- [10] Jack Forman, Mustafa Doga Dogan, Hamilton Forsythe, and Hiroshi Ishii. 2020. DefeXTiles: 3D Printing Quasi-Woven Fabric via Under-Extrusion. In *Proceedings of the 33rd Annual ACM Symposium on User Interface Software and Technology* (UIST ’20). Association for Computing Machinery, New York, NY, USA, 1222–1233. <https://doi.org/10.1145/3379337.3415876>
- [11] Antonio Franchi, Luigi Freda, Giuseppe Oriolo, and Marilena Vendittelli. 2009. The Sensor-based Random Graph Method for Cooperative Robot Exploration. *IEEE/ASME Transactions on Mechatronics* 14, 2 (2009), 163–175. <https://doi.org/10.1109/TMECH.2009.2013617>
- [12] Jun Gong, Olivia Seow, Cedric Honnet, Jack Forman, and Stefanie Mueller. 2021. MetaSense: Integrating Sensing Capabilities into Mechanical Metamaterial. In *The 34th Annual ACM Symposium on User Interface Software and Technology* (Virtual Event, USA) (UIST ’21). Association for Computing Machinery, New York, NY, USA, 1063–1073. <https://doi.org/10.1145/3472749.3474806>
- [13] Liang He, Huaishu Peng, Michelle Lin, Ravikanth Konjeti, François Guimbretière, and Jon E. Froehlich. 2019. Ondulé: Designing and Controlling 3D Printable Springs. In *Proceedings of the 32nd Annual ACM Symposium on User Interface Software and Technology* (New Orleans, LA, USA) (UIST ’19). Association for Computing Machinery, New York, NY, USA, 739–750. <https://doi.org/10.1145/3332165.3347951>

- [14] Liang He, Xia Su, Huaishu Peng, Jeffrey Ian Lipton, and Jon E. Froehlich. 2022. Kinergy: Creating 3D Printable Motion Using Embedded Kinetic Energy. In *Proceedings of the 35th Annual ACM Symposium on User Interface Software and Technology* (Bend, OR, USA) (UIST '22). Association for Computing Machinery, New York, NY, USA, Article 69, 15 pages. <https://doi.org/10.1145/3526113.3545636>
- [15] Huajie Hong, Jabran Ali, and Lei Ren. 2018. A review on topological Architecture and Design Methods of Cable-driven Mechanism. *Advances in Mechanical Engineering* 10, 5 (2018), 1687814018774186.
- [16] Alexandra Ion, Johannes Frohnhofer, Ludwig Wall, Robert Kovacs, Mirela Alistar, Jack Lindsay, Pedro Lopes, Hsiang-Ting Chen, and Patrick Baudisch. 2016. Metamaterial Mechanisms. In *Proceedings of the 29th Annual Symposium on User Interface Software and Technology* (Tokyo, Japan) (UIST '16). Association for Computing Machinery, New York, NY, USA, 529–539. <https://doi.org/10.1145/2984511.2984540>
- [17] Alexandra Ion, David Lindbauer, Philipp Herholz, Marc Alexa, and Patrick Baudisch. 2019. Understanding Metamaterial Mechanisms. In *Proceedings of the 2019 CHI Conference on Human Factors in Computing Systems* (Glasgow, Scotland UK) (CHI '19). Association for Computing Machinery, New York, NY, USA, 1–14. <https://doi.org/10.1145/3290605.3300877>
- [18] Yunwoo Jeong, Han-Jong Kim, and Tek-Jin Nam. 2018. Mechanism Perforboard: An Augmented Reality Environment for Linkage Mechanism Design and Fabrication. In *Proceedings of the 2018 CHI Conference on Human Factors in Computing Systems* (Montreal QC, Canada) (CHI '18). Association for Computing Machinery, New York, NY, USA, 1–11. <https://doi.org/10.1145/3173574.3173985>
- [19] Han-Jong Kim, Yunwoo Jeong, Ju-Whan Kim, and Tek-Jin Nam. 2018. A Prototyping Tool for Kinetic Mechanism Design and Fabrication: Developing and Deploying m.Sketch for Science, Technology, Engineering, the Arts, and Mathematics Education. *Advances in Mechanical Engineering* 10, 12 (Dec. 2018), 168781401880410. <https://doi.org/10.1177/1687814018804104>
- [20] Jinha Lee, Rehmi Post, and Hiroshi Ishii. 2011. ZeroN: Mid-air Tangible Interaction Enabled by Computer Controlled Magnetic Levitation. In *Proceedings of the 24th annual ACM symposium on User interface software and technology*. 327–336.
- [21] Changsheng Li, Xiaoyi Gu, and Hongliang Ren. 2017. A Cable-Driven Flexible Robotic Grasper With Lego-Like Modular and Reconfigurable Joints. *IEEE/ASME Transactions on Mechatronics* 22, 6 (2017), 2757–2767. <https://doi.org/10.1109/TMECH.2017.2765081>
- [22] Jian Li, Sheldon Andrews, Krisztian G Birkas, and Paul G Kry. 2017. Task-based Design of Cable-driven Articulated Mechanisms. In *Proceedings of the 1st Annual ACM Symposium on Computational Fabrication*. 1–12.
- [23] Jiaji Li, Mingming Li, Junzhe Ji, Deying Pan, Yitao Fan, Kuangqi Zhu, Yue Yang, Zihan Yan, Lingyun Sun, Ye Tao, and Guanyun Wang. 2023. All-in-One Print: Designing and 3D Printing Dynamic Objects Using Kinematic Mechanism Without Assembly. In *Proceedings of the 2023 CHI Conference on Human Factors in Computing Systems* (Hamburg, Germany) (CHI '23). Association for Computing Machinery, New York, NY, USA, Article 689, 15 pages. <https://doi.org/10.1145/3544548.3581440>
- [24] Yuyu Lin, Jesse T Gonzalez, Zhitong Cui, Yash Rajeev Banka, and Alexandra Ion. 2024. ConeAct: A Multistable Actuator for Dynamic Materials. In *Proceedings of the CHI Conference on Human Factors in Computing Systems*. 1–16.
- [25] Min Liu, Yunbo Zhang, Jing Bai, Yuanzhi Cao, Jeffrey M. Alperovich, and Karthik Ramani. 2017. WireFab: Mix-Dimensional Modeling and Fabrication for 3D Mesh Models. In *Proceedings of the 2017 CHI Conference on Human Factors in Computing Systems* (Denver, Colorado, USA) (CHI '17). Association for Computing Machinery, New York, NY, USA, 965–976. <https://doi.org/10.1145/3025453.3025619>
- [26] Eric MacDonald and Ryan Wicker. 2016. Multiprocess 3D Printing for Increasing Component Functionality. *Science* 353, 6307 (2016), aaf2093. <https://doi.org/10.1126/science.aaf2093> arXiv:<https://www.science.org/doi/pdf/10.1126/science.aaf2093>
- [27] Vittorio Megaro, Espen Knoop, Andrew Spielberg, David IW Levin, Wojciech Matusik, Markus Gross, Bernhard Thomaszewski, and Moritz Bächer. 2017. Designing Cable-driven Actuation Networks for Kinematic Chains and Trees. In *Proceedings of the ACM SIGGRAPH/Eurographics symposium on computer animation*. 1–10.
- [28] Vittorio Megaro, Jonas Zehnder, Moritz Bächer, Stelian Coros, Markus H Gross, and Bernhard Thomaszewski. 2017. A Computational Design Tool for Compliant Mechanisms. *ACM Trans. Graph.* 36, 4 (2017), 82–1.
- [29] Takafumi Morita, Ziyuan Jiang, Kanon Aoyama, Ayato Minaminosono, Yu Kuwajima, Naoki Hosoya, Shingo Maeda, and Yasuaki Kakehi. 2023. InflatableMod: Untethered and Reconfigurable Inflatable Modules for Tablet-sized Pneumatic Physical Interfaces. In *Proceedings of the 2023 CHI Conference on Human Factors in Computing Systems*. 1–15.
- [30] Takafumi Morita, Yu Kuwajima, Ayato Minaminosono, Shingo Maeda, and Yasuaki Kakehi. 2022. HydroMod: Constructive Modules for Prototyping Hydraulic Physical Interfaces. In *Proceedings of the 2022 CHI Conference on Human Factors in Computing Systems*. 1–14.
- [31] Stefanie Mueller, Sangha Im, Serafima Gurevich, Alexander Teibrich, Lisa Pfisterer, François Guimbretière, and Patrick Baudisch. 2014. WirePrint: 3D Printed Previews for Fast Prototyping. In *Proceedings of the 27th Annual ACM Symposium on User Interface Software and Technology* (Honolulu, Hawaii, USA) (UIST '14). Association for Computing Machinery, New York, NY, USA, 273–280. <https://doi.org/10.1145/2642918.2647359>
- [32] Sachith Muthukumarana, Moritz Alexander Messerschmidt, Denys J.C. Matthies, Jürgen Steimle, Philipp M. Scholl, and Suranga Nanayakkara. 2021. ClothTiles: A Prototyping Platform to Fabricate Customized Actuators on Clothing using 3D Printing and Shape-Memory Alloys. In *Proceedings of the 2021 CHI Conference on Human Factors in Computing Systems* (CHI '21). Association for Computing Machinery, New York, NY, USA, 1–12. <https://doi.org/10.1145/3411764.3445613>
- [33] Koya Narumi, Kazuki Koyama, Kai Suto, Yuta Noma, Hiroki Sato, Tomohiro Tachi, Masaaki Sugimoto, Takeo Igarashi, and Yoshihiro Kawahara. 2023. Inkjet 4D Print: Self-folding Tessellated Origami Objects by Inkjet UV Printing. *ACM Trans. Graph.* 42, 4, Article 117 (jul 2023), 13 pages. <https://doi.org/10.1145/3592409>
- [34] Koya Narumi, Hiroki Sato, Kenichi Nakahara, Young ah Seong, Kunihiko Morinaga, Yasuaki Kakehi, Ryuma Niiyama, and Yoshihiro Kawahara. 2020. Liquid Pouch Motors: Printable Planar Actuators Driven by Liquid-to-gas Phase Change for Shape-changing Interfaces. *IEEE Robotics and Automation Letters* 5, 3 (2020), 3915–3922.
- [35] Negin Nikafrooz and Alexander Leonessa. 2021. A Single-Actuated, Cable-Driven, and Self-Contained Robotic Hand Designed for Adaptive Grasps. *Robotics* 10, 4 (2021). <https://doi.org/10.3390/robotics10040109>
- [36] Yuta Noma, Koya Narumi, Fuminori Okuya, and Yoshihiro Kawahara. 2020. Pop-up Print: Rapidly 3D Printing Mechanically Reversible Objects in the Folded State. In *Proceedings of the 33rd Annual ACM Symposium on User Interface Software and Technology* (Virtual Event, USA) (UIST '20). Association for Computing Machinery, New York, NY, USA, 58–70. <https://doi.org/10.1145/3379337.3415853>
- [37] Yuta Noma, Koya Narumi, Fuminori Okuya, and Yoshihiro Kawahara. 2020. Pop-up Print: Rapidly 3D Printing Mechanically Reversible Objects in the Folded State. In *Proceedings of the 33rd Annual ACM Symposium on User Interface Software and Technology*. ACM, Virtual Event USA, 58–70. <https://doi.org/10.1145/3379337.3415853>
- [38] Jifei Ou, Gershon Dublon, Chin-Yi Cheng, Felix Heibeck, Karl Willis, and Hiroshi Ishii. 2016. Cillia: 3D Printed Micro-Pillar Structures for Surface Texture, Actuation and Sensing. In *Proceedings of the 2016 CHI Conference on Human Factors in Computing Systems*. ACM, San Jose California USA, 5753–5764. <https://doi.org/10.1145/2858036.2858257>
- [39] Athina Panotopoulou, Valkyrie Savage, and Daniel Lee Ashbrook. 2024. Threa-D Printing Tunable Bistable Mechanisms. In *Adjunct Proceedings of the 9th ACM Symposium on Computational Fabrication* (Aarhus, Denmark) (SCF Adjunct '24). Association for Computing Machinery, New York, NY, USA, Article 16, 3 pages. <https://doi.org/10.1145/3665662.3673272>
- [40] Huaishu Peng, François Guimbretière, James McCann, and Scott Hudson. 2016. A 3D Printer for Interactive Electromagnetic Devices. In *Proceedings of the 29th Annual Symposium on User Interface Software and Technology* (Tokyo, Japan) (UIST '16). Association for Computing Machinery, New York, NY, USA, 553–562. <https://doi.org/10.1145/2984511.2984523>
- [41] Franklin Pezutti-Dyer and Leah Buechley. 2022. Extruder-Turtle: A Library for 3D Printing Delicate, Textured, and Flexible Objects. In *Sixteenth International Conference on Tangible, Embedded, and Embodied Interaction*. ACM, Daejeon Republic of Korea, 1–9. <https://doi.org/10.1145/3490149.3501312>
- [42] Katy Pieri, Bailey M. Felix, Teng Zhang, Pranav Soman, and James H. Henderson. 2023. Printing Parameters of Fused Filament Fabrication Affect Key Properties of Four-Dimensional Printed Shape-Memory Polymers. *3D Printing and Additive Manufacturing* 10, 2 (2023), 279–288. <https://doi.org/10.1089/3dp.2021.0072> arXiv:<https://doi.org/10.1089/3dp.2021.0072>
- [43] Stefan Pillwein, Johanna Kübert, Florian Rist, and Przemyslaw Musialski. 2020. Design and Fabrication of Elastic Geodesic Grid Structures. In *Proceedings of the 5th Annual ACM Symposium on Computational Fabrication* (Virtual Event, USA) (SCF '20). Association for Computing Machinery, New York, NY, USA, Article 2, 11 pages. <https://doi.org/10.1145/3424630.3425412>
- [44] Sen Qian, Bin Zi, Wei-Wei Shang, and Qing-Song Xu. 2018. A Review on Cable-driven Parallel Robots. *Chinese Journal of Mechanical Engineering* 31, 1 (Aug. 2018), 66. <https://doi.org/10.1186/s10033-018-0267-9>
- [45] Michael L. Rivera, Melissa Moukperian, Daniel Ashbrook, Jennifer Mankoff, and Scott E. Hudson. 2017. Stretching the Bounds of 3D Printing with Embedded Textiles. In *Proceedings of the 2017 CHI Conference on Human Factors in Computing Systems* (Denver, Colorado, USA) (CHI '17). Association for Computing Machinery, New York, NY, USA, 497–508. <https://doi.org/10.1145/3025453.3025460>
- [46] João Cavalcanti Santos, Marc Gouttefarde, and Ahmed Chemori. 2022. A Non-linear Model Predictive Control for the Position Tracking of Cable-Driven Parallel Robots. *IEEE Transactions on Robotics* 38, 4 (2022), 2597–2616. <https://doi.org/10.1109/TRO.2022.3152705>
- [47] Harpreet Sareen, Udayan Umapathi, Patrick Shin, Yasuaki Kakehi, Jifei Ou, Hiroshi Ishii, and Pattie Maes. 2017. Printflatables: Printing Human-Scale, Functional and Dynamic Inflatable Objects. In *Proceedings of the 2017 CHI Conference on Human Factors in Computing Systems* (Denver, Colorado, USA) (CHI '17). Association for Computing Machinery, New York, NY, USA, 3669–3680.



- <https://doi.org/10.1145/3025453.3025898>
- [48] Christian Schumacher, Bernd Bickel, Jan Rys, Steve Marschner, Chiara Daraio, and Markus Gross. 2015. Microstructures to Control Elasticity in 3D Printing. *ACM Trans. Graph.* 34, 4, Article 136 (jul 2015), 13 pages. <https://doi.org/10.1145/2766926>
- [49] Herschel Shapiro. 2022. Herschel Shapiro's Artworks. <https://www.youtube.com/@HerschelShapiro>. Accessed: 2024-09-15.
- [50] Shouhei Shirafuji, Shuhei Ikemoto, and Koh Hosoda. 2016. Designing noncircular pulleys to realize target motion between two joints. *IEEE/ASME Transactions on Mechatronics* 22, 1 (2016), 487–497.
- [51] Ali Shtarbanov. 2021. Flowio development platform—the pneumatic “raspberry pi” for soft robotics. In *Extended abstracts of the 2021 CHI conference on human factors in computing systems*. 1–6.
- [52] Lingyun Sun, Jiayi Li, Yu Chen, Yue Yang, Zhi Yu, Danli Luo, Jianzhe Gu, Lining Yao, Ye Tao, and Guanyun Wang. 2021. FlexTruss: A Computational Threading Method for Multi-Material, Multi-Form and Multi-Use Prototyping. In *Proceedings of the 2021 CHI Conference on Human Factors in Computing Systems (Yokohama, Japan) (CHI '21)*. Association for Computing Machinery, New York, NY, USA, Article 432, 12 pages. <https://doi.org/10.1145/3411764.3445311>
- [53] Lingyun Sun, Jiayi Li, Junzhe Ji, Deying Pan, Mingming Li, Kuangqi Zhu, Yitao Fan, Yue Yang, Ye Tao, and Guanyun Wang. 2022. X-Bridges: Designing Tunable Bridges to Enrich 3D Printed Objects' Deformation and Stiffness. In *Proceedings of the 35th Annual ACM Symposium on User Interface Software and Technology (Bend, OR, USA) (UIST '22)*. Association for Computing Machinery, New York, NY, USA, Article 20, 12 pages. <https://doi.org/10.1145/3526113.3545710>
- [54] Lingyun Sun, Jiayi Li, Mingming Li, Yitao Fan, Yu Chen, Deying Pan, Yue Yang, Junzhe Ji, Ye Tao, and Guanyun Wang. 2021. 3DP-Ori: Bridging-Printing Based Origami Fabrication Method with Modifiable Haptic properties. In *Adjunct Proceedings of the 34th Annual ACM Symposium on User Interface Software and Technology (Virtual Event, USA) (UIST '21 Adjunct)*. Association for Computing Machinery, New York, NY, USA, 74–77. <https://doi.org/10.1145/3474349.3480233>
- [55] Saiganesh Swaminathan, Kadri Bugra Ozutemiz, Carmel Majidi, and Scott E. Hudson. 2019. FiberWire: Embedding Electronic Function into 3D Printed Mechanically Strong, Lightweight Carbon Fiber Composite Objects. In *Proceedings of the 2019 CHI Conference on Human Factors in Computing Systems (Glasgow, Scotland Uk) (CHI '19)*. Association for Computing Machinery, New York, NY, USA, 1–11. <https://doi.org/10.1145/3290605.3300797>
- [56] Kazutoshi Tanaka and Masashi Hamaya. 2023. Twist Snake: Plastic table-top cable-driven robotic arm with all motors located at the base link. In *2023 IEEE International Conference on Robotics and Automation (ICRA)*. 7345–7351. <https://doi.org/10.1109/ICRA48891.2023.10160995>
- [57] Bernhard Thomaszewski, Stelian Coros, Damien Gauge, Vittorio Megaro, Eitan Grinspun, and Markus Gross. 2014. Computational Design of Linkage-Based Characters. *ACM Trans. Graph.* 33, 4, Article 64 (jul 2014), 9 pages. <https://doi.org/10.1145/2601097.2601143>
- [58] Guanyun Wang, Tingyu Cheng, Youngwook Do, Humphrey Yang, Ye Tao, Jianzhe Gu, Byoungkwon An, and Lining Yao. 2018. Printed Paper Actuator: A Low-cost Reversible Actuation and Sensing Method for Shape Changing Interfaces. In *Proceedings of the 2018 CHI Conference on Human Factors in Computing Systems*. ACM, Montreal QC Canada, 1–12. <https://doi.org/10.1145/3173574.3174143>
- [59] Guanyun Wang, Ye Tao, Ozguc Bertug Capunaman, Humphrey Yang, and Lining Yao. 2019. A-Line: 4D Printing Morphing Linear Composite Structures. In *Proceedings of the 2019 CHI Conference on Human Factors in Computing Systems (Glasgow, Scotland Uk) (CHI '19)*. Association for Computing Machinery, New York, NY, USA, 1–12. <https://doi.org/10.1145/3290605.3300656>
- [60] Ruiqin Wang, Hao Wu, and Jian S. Dai. 2024. A Novel Bio-Inspired Quadruped Crawling Robot with Movable Waist. In *2024 6th International Conference on Reconfigurable Mechanisms and Robots (ReMAR)*. 218–223. <https://doi.org/10.1109/ReMAR61031.2024.10617730>
- [61] Yue Yang, Lei Ren, Chuang Chen, Bin Hu, Zhuoyi Zhang, Xinyan Li, Yanchen Shen, Kuangqi Zhu, Junzhe Ji, Yuyang Zhang, Yongbo Ni, Jiayi Wu, Qi Wang, Jiang Wu, Lingyun Sun, Ye Tao, and Guanyun Wang. 2024. SnapInflatables: Designing Inflatables with Snap-through Instability for Responsive Interaction. In *Proceedings of the CHI Conference on Human Factors in Computing Systems (Honolulu, HI, USA) (CHI '24)*. Association for Computing Machinery, New York, NY, USA, Article 342, 15 pages. <https://doi.org/10.1145/3613904.3642933>
- [62] Lining Yao, Ryuma Niiyama, Jifei Ou, Sean Follmer, Clark Della Silva, and Hiroshi Ishii. 2013. PneuUI: pneumatically actuated soft composite materials for shape changing interfaces. In *Proceedings of the 26th annual ACM symposium on User interface software and Technology*. 13–22.
- [63] Mahmoud Zarebidoki, Jaspreet Singh Dhupia, and Weiliang Xu. 2022. A review of cable-driven parallel robots: Typical configurations, analysis techniques, and control methods. *IEEE Robotics & Automation Magazine* 29, 3 (2022), 89–106.
- [64] Wensi Zhang, Barnabas Gavin Cangan, Thomas Buchner, Alexander M Kübler, Ramon Asmus, and Robert K Katzschmann. 2024. Task-defined Pulley Design for Nonlinearly Coupled Tendon-driven Actuation. In *2024 IEEE 7th International Conference on Soft Robotics (RoboSoft)*. IEEE, 220–227.
- [65] Amit Zoran. 2013. Hybrid basketry: interweaving digital practice within contemporary craft. In *ACM SIGGRAPH 2013 Art Gallery (Anaheim, California) (SIGGRAPH '13)*. Association for Computing Machinery, New York, NY, USA, 324–331. <https://doi.org/10.1145/2503649.2503651>

## A PRINTING SETTINGS FOR DIFFERENT MODEL OF 3D PRINTER

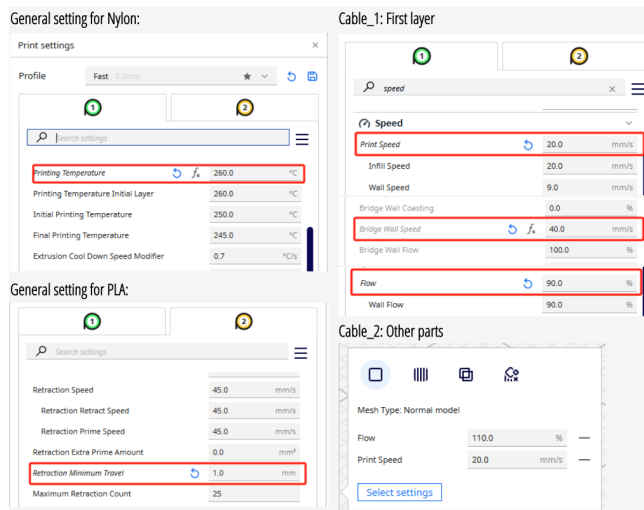


Figure 24: Settings for Ultimaker 3 and S5

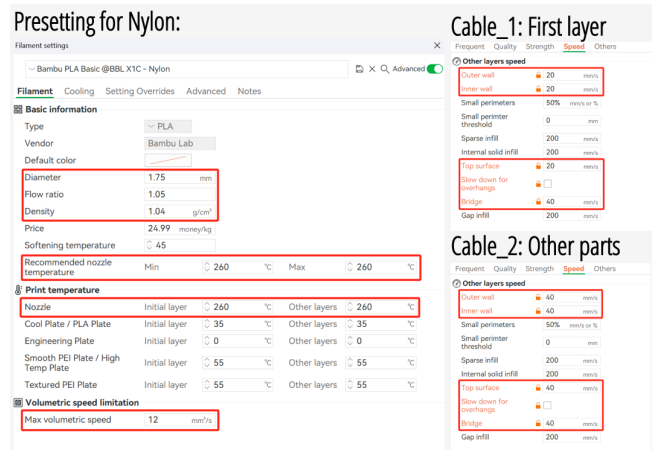


Figure 25: Settings for Bambu X1